
Article:
Llewelyn, S.C.H., Christofidou, K.A. orcid.org/0000-0002-8064-5874, Araullo-Peters, V.J. et al. (4 more authors) (2017) The effect of Ni:Co ratio on the elemental phase partitioning in γ-γ′ Ni-Co-Al-Ti-Cr alloys. Acta Materialia, 131. pp. 296-304. ISSN 1359-6454

https://doi.org/10.1016/j.actamat.2017.03.067

Acta Materialia 131 (2017) 296–304

Contents lists available at ScienceDirect

Acta Materialia

journal homepage: www.elsevier.com/locate/actamat

Full length article

The effect of Ni:Co ratio on the elemental phase partitioning in γ-γ′ Ni-Co-Al-Ti-Cr alloys

S.C.H. Llewelyn [a], K.A. Christofidou [a], V.J. Araullo-Peters [b], N.G. Jones [a], M.C. Hardy [c], E.A. Marquis [b], H.J. Stone [a, *]

[a] Department of Materials Science and Metallurgy, University of Cambridge, 27 Charles Babbage Road, Cambridge, CB3 0FS, UK
[b] Department of Materials Science and Engineering, University of Michigan, Ann Arbor, MI, 48109, United States
[c] Rolls-Royce plc, PO Box 31, Derby, DE24 8BJ, UK

ARTICLE INFO

Article history:
Received 3 February 2017
Received in revised form
23 March 2017
Accepted 26 March 2017
Available online 28 March 2017

Keywords:
Atom-probe tomography
Nickel
Cobalt
Superalloys
Phase composition

ABSTRACT

Atom probe tomography has been used to characterise the effect of varying Ni:Co ratio on elemental phase partitioning at 800 °C in γ-γ′ alloys derived from the Ni-Co-Al-Ti-Cr system. In all alloys tested, Al and Ti were found to partition preferentially to the γ′ phase, whereas Co and Cr partitioned preferentially to the γ phase. However, above a critical Co content (~19 at.%), the extent of partitioning of Al and Ti to the γ′ phase reduced. Conversely, Cr partitioned more strongly to the γ phase with Co additions of up to ~19 at.%, above which this preferential segregation was less pronounced. This non-monotonic trend of elemental partitioning behaviour with increasing Co concentration was attributed to a transition in the chemistry of the $L1_2$ γ′ phase from $Ni_3(Ti, Al)$ to $(Ni, Co)_3(Ti, Al)$ and thus to a change in its solute solubility.

1. Introduction

In the drive to make air travel more sustainable, aero-engines must operate with greater efficiency and one method of achieving this is to increase the temperature of the gas entering the turbine. This imposes more stringent service conditions on the alloys from which aero-engine turbine components are fabricated, requiring new higher performance alloys to be developed that can sustain these higher operating temperatures. Currently, the polycrystalline Ni-based superalloys used for many such components typically comprise a Ni-rich solid solution (γ) exhibiting the face-centred cubic (A1) crystal structure strengthened by coherent particles of an intermetallic phase, $Ni_3(Al, Ti)$ (γ′), possessing the $L1_2$ superlattice structure [1]. One method by which superalloys can be designed with higher proof strength and greater creep resistance is through increasing the volume fraction of the strengthening γ′ phase for a given temperature [2,3]. This can be readily achieved through increasing the concentration of γ′-forming elements such as Al and Ti. Ti additions also offer the benefit of increasing the anti-phase boundary energy of the γ′ phase whilst not negatively impacting alloy density [4]. However, excessive Ti additions increase the propensity to form the Ni_3Ti (η) phase, which has the $D0_{24}$ crystal structure and is generally considered deleterious to alloy properties [5]. This issue may be overcome through the use of Co-Ti co-additions [6], enabling new superalloy compositions with improved high temperature strength and creep resistance.

In the binary Co-Ti phase diagram [7] a two-phase field exists above 600 °C between an A1 Co-rich solid solution and the $L1_2$ Co_3Ti intermetallic phase. As with Ni_3Al, the monolithic Co_3Ti compound exhibits an increase in proof stress with increasing temperature [8]. Indeed, the strength of Co_3Ti has been shown to exceed that of Ni_3Al at temperatures greater than 730 °C [9] and is thus anticipated to confer improved high temperature strength over conventional superalloys. Furthermore, the Co_3Ti intermetallic has the advantage of relatively low cost and low density compared with other candidate $L1_2$ intermetallics such as $Co_3(Al, W)$. Unfortunately, alloys based on the Co-Co_3Ti two-phase field are not currently considered as viable alternatives to Ni-based superalloys as their microstructures are often unstable, precipitating detrimental intermetallic phases and exhibiting discontinuous reaction products at elevated temperature [10–12]. A further barrier to the

* Corresponding author.
E-mail address: hjs1002@cam.ac.uk (H.J. Stone).

http://dx.doi.org/10.1016/j.actamat.2017.03.067

commercial use of Co-Co_3Ti based alloys is the low solvus temperature of the γ′-Co_3Ti, which typically lies in the range of 815–872 °C [13]. However, simultaneous additions of Co and Ti to conventional Ni-based superalloys have been shown to enable the development of (Ni, Co)-based superalloys that exhibit improved high temperature properties over conventional superalloys.

A partial phase diagram of the quaternary Ni-Al-Co-Ti system has been experimentally derived for temperatures between 750 and 1100 °C [14–16]. It has been reported that a continuous $L1_2$ phase field exists between Ni_3Al and Co_3Ti (γ′) along their near-stoichiometric compositions and that a continuous A1 phase field (γ) exists between the Ni-rich and Co-rich vertices of the phase diagram. Furthermore, for this range of temperatures, a continuous two phase field of γ and γ′ has been shown to exist between the Ni-Ni_3Al and Co-Co_3Ti equilibria, such that any alloy composition within this two-phase field may produce the desirable A1-$L1_2$ microstructure [14–16]. Consistent with this result, a number of studies have shown that, by incorporating elevated concentrations of Co and Ti into commercial Ni-based superalloy compositions, it is possible to achieve a γ-γ′ microstructure that possesses superior high temperature strength and creep resistance compared with conventional Ni-based superalloys [4,13,17–19]. This effect has been attributed to several mechanisms, most notably to an increase in γ′ volume fraction as well as to an increase in the solid solution hardening of γ and γ′ by Co and Ti respectively [17,19].

Critically, the relative concentrations of the different alloying elements in Ni-based superalloys determine the elemental partitioning behaviour between the γ and γ′ phases and, therefore, the properties of the alloy. Previous studies have shown that Co partitions preferentially to the γ phase and has a significant influence on the solubility of other alloying elements in the γ and γ′ phases of Ni-based superalloys [19–22]. For example, additions of Co have been found to increase the volume fraction of γ′ in commercial Ni-based superalloys [20,23–25] and this has been attributed to the effect that Co has in reducing the solubility of Al and Ti in the γ solid solution [21,23]. This is consistent with a recent study by Oni et al. [22], who used atom probe tomography to highlight the differences in elemental partitioning between the γ and γ′ phases in three Ni-Al-Co-Ti alloys with varying Co and Ti content.

Chromium is a critical addition in polycrystalline Ni-based superalloys as it imparts resistance to oxidation and hot corrosion via the formation of a protective (diffusion-resistant) Cr_2O_3-rich scale [2]. However, high Cr concentrations in the alloy increase the propensity to form deleterious topologically close-packed (TCP) intermetallic phases such as σ [1]. Therefore, it is desirable that the partitioning of Ni, Al, Co and Ti between the γ and γ′ phases is assessed in the presence of Cr, as its concentration in the γ phase must be optimised to provide environmental resistance whilst also retaining microstructural stability. Elemental partitioning between the γ and γ′ phases in such quinary alloys has been shown to affect their microstructure and resultant properties. Specifically, differences observed in the hardness of γ-γ′ Ni-Co-Al-Ti-Cr alloys have been attributed to the effect of the Ni:Co ratio on the partitioning of the other elements [26]. Given the importance of elemental partitioning on the microstructure and properties of superalloys, an improved understanding of the phase equilibria is therefore critical if optimised compositions are to be designed. To this end, this study aims to elucidate the influence of the Ni:Co ratio on the elemental partitioning behaviour in alloys comprising Ni-Al-Co-Ti as well as Cr, as the latter is a critical addition in polycrystalline superalloys intended for service below 800 °C due to its ability to impart oxidation and hot corrosion resistance.

2. Experimental procedure

2.1. Material and heat treatment

The series of model superalloys investigated in the present study was based on the $(Ni, Co)_{75}Al_5Ti_5Cr_{15}$ (at.%) system in which the Ni:Co concentration ratio was varied from 1:0 to 1:3, Table 1. The concentration ratio of Al:Ti was kept at one to allow systematic assessment of the influence of Co on the partitioning of solute elements between the γ and γ′ phases. Additionally, the total Al + Ti content was fixed at 10 at.% to achieve comparable γ′ volume fractions in the alloys. The alloys were named according to their nominal at.% Co.

Vacuum arc melting was used to fabricate polycrystalline samples of the seven alloys from raw elements of at least 99.9% purity. Thermal analysis of the as-cast alloys was performed using differential scanning calorimetry (DSC) to determine the critical phase transformation temperatures, knowledge of which was required for the selection of suitable homogenising temperatures. DSC tests were performed using a Netzsch 404 heat-flux calorimeter operating at temperatures of up to 1450 °C with a heating rate of 10 °C min^{-1}. The alloys were sealed in quartz tubes under an Ar atmosphere before being subjected to a homogenisation heat treatment in the single γ phase field at 1250 °C for 24 h to minimise the effect of casting-induced micro-segregation. The homogenisation heat treatment temperature was chosen to be higher than the γ′ solvus temperatures of all of the alloys but sufficiently lower than their solidus temperatures to avoid incipient melting. Following the homogenisation heat treatment, all alloys were subjected to an ageing heat treatment at 800 °C for 1000 h to attain the thermodynamically stable phase distributions at this temperature. The alloy specimens were then air-cooled.

2.2. Scanning electron microscopy (SEM)

Alloy specimens in the as-homogenised and fully aged conditions were mounted in conductive Bakelite and prepared for metallographical examination by grinding using wet SiC abrasive paper. They were then polished using progressively finer diamond suspensions down to 1 μm. Specimens were subsequently electrolytically etched using a 10% phosphoric acid solution in order to dissolve the γ matrices and to highlight the γ′ particles. Microstructural examination of the alloys was performed using an FEI Nova NanoSEM 450 scanning electron microscope in secondary electron mode. Energy dispersive X-ray spectroscopy (EDS) was performed using a Bruker XFlash 6 solid state EDS system to identify the overall compositions of the alloys, Table 1, which were obtained from a minimum of 5 large area scans of at least 0.5 × 0.5 mm in size.

2.3. Differential scanning calorimetry (DSC)

DSC was performed to determine the γ′ solvus, solidus and liquidus temperatures of the seven model superalloys after the ageing heat treatment of 800 °C for 1000 h. Small discs of 5 mm in diameter and 1 mm in thickness were extracted from each alloy in the fully aged condition using spark erosion. DSC tests on these aged alloy specimens were performed as for the as-cast alloy specimens using a Netzsch 404 heat-flux calorimeter operating at temperatures of up to 1450 °C with a heating rate of 10 °C min^{-1}. Data analysis was performed using Igor Pro 6.3 software [27].

Table 1
Nominal chemical compositions of the alloys, together with the measured compositions and their standard deviations (σ) for the alloys in the fully aged condition using SEM-EDS.

Alloy	Nominal composition (at.%)					Measured composition (at.%)									
	Ni	Co	Al	Ti	Cr	Ni	±σ	Co	±σ	Al	±σ	Ti	±σ	Cr	±σ
0Co	75.0	0.0	5.0	5.0	15.0	74.34	0.06	–	–	5.46	0.07	5.35	0.06	14.85	0.09
9Co	65.6	9.4	5.0	5.0	15.0	64.9	0.3	9.4	0.3	5.41	0.17	5.4	0.2	14.91	0.10
19Co	56.3	18.8	5.0	5.0	15.0	55.9	0.6	18.85	0.15	5.2	0.9	5.21	0.10	14.83	0.11
28Co	46.9	28.1	5.0	5.0	15.0	46.5	0.2	28.42	0.14	5.24	0.16	5.31	0.09	14.54	0.15
38Co	37.5	37.5	5.0	5.0	15.0	37.55	0.04	37.88	0.06	4.69	0.03	5.13	0.06	14.76	0.06
47Co	28.1	46.9	5.0	5.0	15.0	27.78	0.19	47.9	0.3	4.91	0.17	4.92	0.18	14.52	0.17
56Co	18.8	56.3	5.0	5.0	15.0	18.89	0.08	57.02	0.14	4.31	0.05	5.06	0.05	14.71	0.05

2.4. Atom probe tomography (APT)

Atom probe tomography (APT) was performed to determine the compositions of the γ and γ′ phases within the seven model superalloys aged at 800 °C for 1000 h. Cuboidal rods (0.5 × 0.5 × 15 mm) were extracted from each alloy in the fully aged condition using electrical discharge machining (EDM). From these rods, specimens suitable for APT analysis were prepared in the form of sharply pointed needles by a rough electropolish using a 25% perchloric acid solution at a voltage of 15–20 V, followed by fine electropolishing using a more dilute perchloric acid solution (2%) at a voltage of 15 V. All APT experiments were carried out using a CAMECA local-electrode atom-probe (LEAP) 4000X HR instrument at the Michigan Center for Materials Characterization. The instrument was operated in the high-voltage pulsing mode with the superimposed pulsing voltage at nominally 20% of the steady-state voltage and a detection efficiency of ~36%. Specimen temperatures were maintained at nominally 50 K. Initial data processing was performed using the CAMECA IVAS 3.6.8 software. Data were subsequently processed to deconvolve the overlapping isotopic peaks. Proximity histograms (proxigrams) were generated from the data acquired, which displayed the atomic fraction of each element as a function of its proximity to the γ/γ′ interface, as defined using an isoconcentration surface of Al and/or Ti. These surfaces were used as reference points for calculating the proxigrams, which were computed 10 nm either side of the interfaces using a 0.5 nm bin size. Error bars displayed represent one standard deviation (σ) and were calculated using: $\sigma = \sqrt{(C_i(1-C_i))/N}$, where C_i is the calculated atomic fraction of each element *i* and N is the total number of atoms in each bin [28]. For each alloy, the mean elemental concentrations in the γ and γ′ phases were quantified using data points away from the interface, where the deviation from the average value was not more than ~1 at.%. The uncertainty associated with these values was taken to be the standard deviation of the elemental concentrations over the range used to calculate the average values.

The elemental concentration data were used to calculate the volume fraction of the γ′ phase in each alloy using the lever rule: $C_i^{alloy} = (C_i^{\gamma} \cdot f^{\gamma'}) + (C_i^{\gamma} \cdot (1 - f^{\gamma'}))$, where C_i^{alloy} is the nominal concentration of element *i* in the alloy, C_i^{γ} and $C_i^{\gamma'}$ are the concentrations of the same element in the γ and γ′ phases respectively and $f^{\gamma'}$ is the volume fraction of γ′ in the alloy. The overall γ′ volume fraction in each alloy was determined by rearranging the lever rule:

$$f^{\gamma'} = \frac{C_i^{alloy} - C_i^{\gamma}}{C_i^{\gamma'} - C_i^{\gamma}}$$

Values for $C_i^{alloy} - C_i^{\gamma}$ were then plotted against values for $C_i^{\gamma'} - C_i^{\gamma}$ for the individual alloying elements and a linear regression analysis performed to determine the line gradient, equivalent to $f^{\gamma'}$.

2.5. Computational modelling

The compositions of the γ and γ′ phases in the quinary Ni-Co-Al-Ti-Cr alloys were calculated by the CALPHAD approach using the Thermo-Calc software with the TCNi8 database. Phase equilibria were calculated for 800 °C without suppressing the formation of any phases. In addition, the equilibrium phase transition temperatures of each alloy were computed using Thermo-Calc with the TCNi8 database.

3. Results

Duplex γ-γ′ microstructures were observed in all alloys in their homogenised condition and following ageing at 800 °C with no other phases observed, Fig. 1. The Co-free alloy, Fig. 1a, and those containing up to 38 at.% Co, Fig. 1b–e, comprised isolated γ′ particles. The 47Co and 56Co alloys, Fig. 1f–g, exhibited elongated γ′ precipitates, suggesting directional coalescence during particle growth. It should be noted that the triangular appearance of the particles in the 47Co alloy, Fig. 1f, was consistent with the sectioning plane being away from {100}.

Fig. 2 shows the volume fraction of the γ′ phase in each alloy as derived from the experimental APT data as a function of the nominal Co content, compared with predicted values determined using Thermo-Calc with the TCNi8 database. The experimental data indicate that the γ′ volume fraction increased slightly with Co additions of up to 19 at.%, with a subsequent decrease in γ′ volume fraction observed as alloy Co content increased further. The modelled predictions of γ′ volume fraction were consistently lower than experimental values.

3.1. Phase transition temperatures

Fig. 3 shows the γ′ solvus, solidus and liquidus temperatures of the aged alloys as a function of the nominal Co content. The experimental data indicate that the solvus temperature of the γ′ phase decreased with increasing Co concentration, consistent with Thermo-Calc predictions for the alloys of higher Co content. The Co concentration appears to have had a less pronounced effect on the experimentally obtained solidus and liquidus temperatures.

3.2. Elemental phase partitioning

Compositional data obtained from the 0Co alloy were used as a baseline to which corresponding data from the quinary (Co-containing) alloys could be compared. Fig. 4a displays a 10 nm slice through the reconstruction of the atom probe sample of the aged Co-free alloy, showing the Ni, Al, Ti and Cr solute distributions where each coloured dot represents one atom of a particular solute

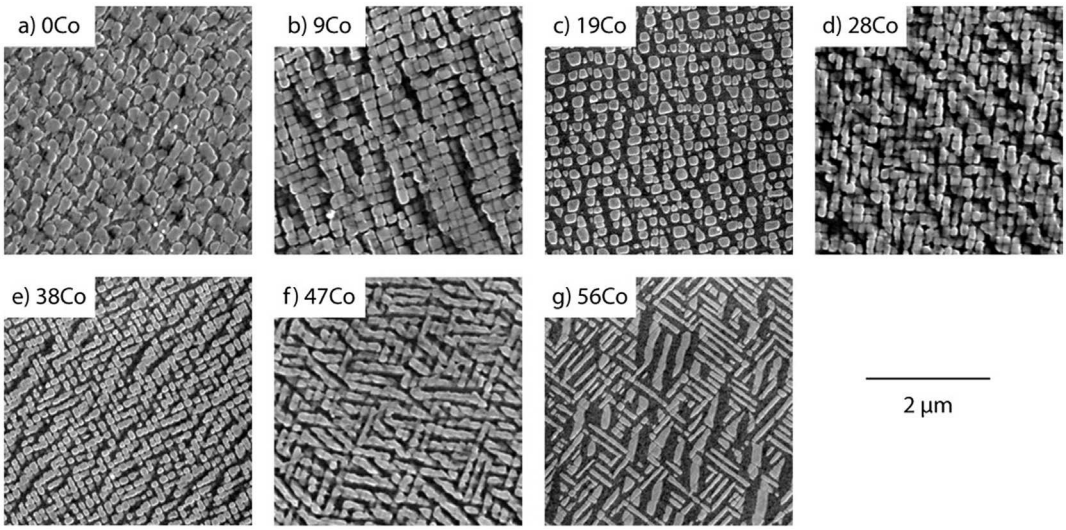

Fig. 1. Secondary electron images of the A1-L1$_2$ microstructure, showing γ′ particles embedded in the γ matrix of alloys: (a) 0Co, (b) 9Co, (c) 19Co, (d) 28Co, (e) 38Co, (f) 47Co and (g) 56Co following ageing at 800 °C for 1000 h.

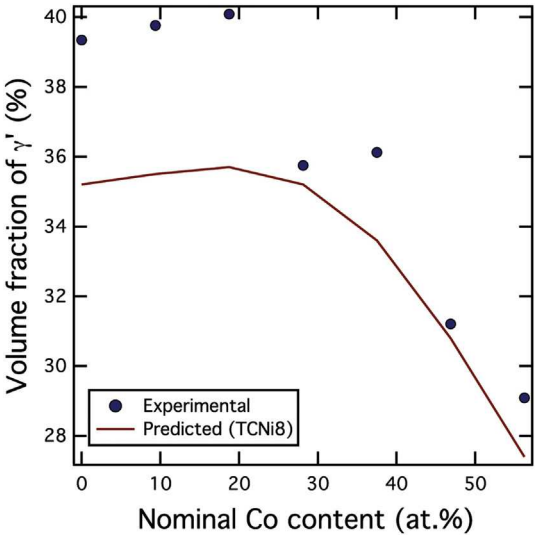

Fig. 2. Volume fraction of the γ′ phase in the Ni-Co-5Al-5Ti-15Cr alloys tested as a function of nominal alloy Co content. Experimental data (markers) are compared with thermodynamic model predictions (solid lines) obtained using Thermo-Calc with the TCNi8 database for 800 °C.

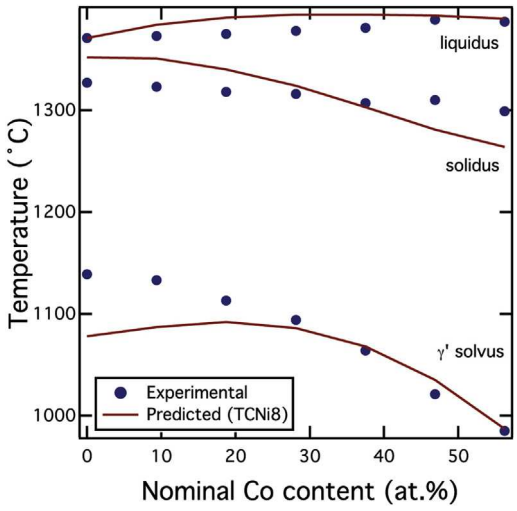

Fig. 3. Liquidus, solidus and γ′ solvus temperatures of the Ni-Co-5Al-5Ti-15Cr alloys as a function of nominal alloy Co content. Experimental data (markers) are compared with thermodynamic model predictions (solid lines) obtained using Thermo-Calc with the TCNi8 database.

species. Two phases were identified, pertaining to γ and γ′ as indicated. The associated proximity histograms are presented in Fig. 4b. It can be seen that the concentrations of Ni in the γ and γ′ phases were similar, although a slight decrease in Ni concentration at the interface was observed. The other elements showed a marked difference in solute concentration between the γ and γ′ phases. The γ phase was enriched with Cr (~23 at.%) and the γ′ phase was enriched with Ti (~11 at.%) and Al (~11 at.%).

Fig. 5a displays a 10 nm slice through the atom probe reconstruction of the aged 56Co alloy, showing the Ni, Ti, Al, Cr and Co solute distributions. It is evident that the γ matrix was rich in Cr and Co and that the γ′ precipitates were rich in Ni, Ti and Al. The corresponding proxigrams shown in Fig. 5b permit an estimate to be obtained for elemental concentration within the γ and γ′ phases. Thus, the γ phase comprised approximately 59 at.% Co and 21 at.% Cr whilst the γ′ phase comprised approximately 30 at.% Ni, 12 at.% Ti and 8 at.% Al. The proxigrams also indicated the presence of a diffuse interface between the γ and γ′ phases approximately 20 nm in width. In the γ phase approaching the interface, there appeared to be a slight enrichment in Co and Cr and depletion in Ni, Ti and Al. This may be attributed to the coarsening of the γ′ precipitates observed in this alloy (Fig. 1g). Figures showing the atom probe reconstructions and proximity histograms pertaining to the other five alloys are available online in supplementary information.

Comparison of Figs. 4 and 5 indicates that the addition of 56 at.% Co to the Ni-Al-Ti-Cr quaternary alloy caused less extensive partitioning of Al than of Ti to the γ′ phase. Increased partitioning of Ni towards the γ′ phase was observed in alloy 56Co compared with alloy 0Co.

Table 2 shows the mean atomic concentrations of elements within the γ and γ′ phases for each alloy, quantified from their respective proxigrams. The elemental partitioning coefficient (k_i) was defined as the ratio of the concentration of element *i* in the γ′

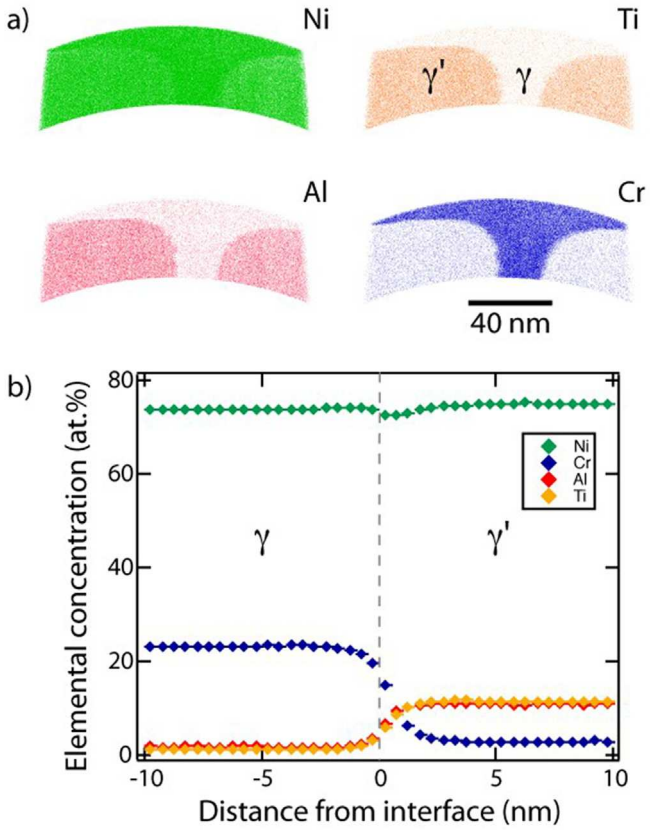

Fig. 4. (a) Atom probe reconstructions of the spatial distributions of Ni, Ti, Al and Cr atoms within a 10 nm slice through the volume analysed of aged **alloy 0Co**. 100% Al (red), 100% Ti (orange), 100% Cr (blue) ions are shown but only 70% Ni (green) ions are shown so that the γ and γ′ phases may be distinguished. (b) Proxigrams showing solute concentration profiles across the γ/γ′ interface. Error bars have been included but are smaller than the symbols used. (For interpretation of the references to colour in this figure legend, the reader is referred to the web version of this article.)

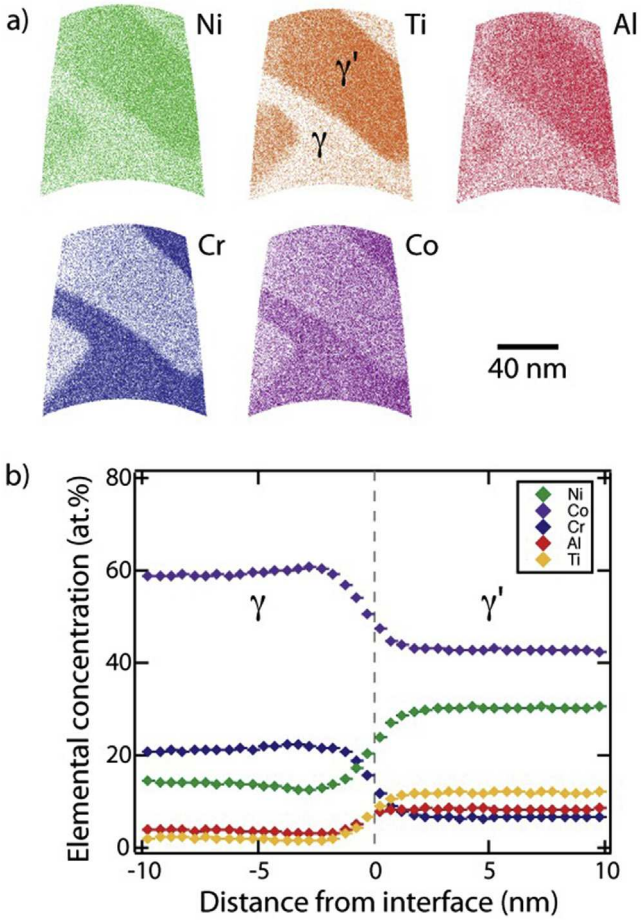

Fig. 5. (a) Atom probe reconstructions of the spatial distributions of Ni, Ti, Al, Cr and Co atoms within a 10 nm slice through the volume analysed of aged **alloy 56Co**. To distinguish the γ phase from the γ′ phase, only a fraction of the ions are shown for each element [10% Ni (green), 30% Al (red), 30% Ti (orange), 20% Cr (blue) and 4% Co (purple)]. (b) Proxigrams showing solute concentration profiles across the γ/γ′ interface. Error bars have been included but are smaller than the symbols used. (For interpretation of the references to colour in this figure legend, the reader is referred to the web version of this article.)

phase ($C_i^{\gamma'}$) to the concentration of the same element in the γ phase (C_i^{γ}) according to:

$$k_i = \frac{C_i^{\gamma'}}{C_i^{\gamma}}$$

This parameter is useful in the assessment of preferential phase partitioning of solutes and is displayed for i = Al, Ti, Ni, Cr and Co in Table 2. As inferred from k_i values in excess of 1, it is apparent that Ti and Al, and to a lesser extent Ni, segregated preferentially to the γ′ phase. At any given alloy Co content, Ti exhibited a higher k_i than Al, suggesting that preferential partitioning to the γ′ phase was higher for Ti than for Al. Conversely, Cr and Co partitioned preferentially to the γ matrix phase in all alloy compositions, as indicated by k_i values of less than unity. The extent of preferential partitioning of individual alloying elements was observed to be highly dependent on the Ni:Co ratio of the alloy.

3.3. Effects of alloying with cobalt

To elucidate how the partitioning of Al, Ti and Cr between the γ and γ′ phases varied with the Ni:Co ratio, the elemental concentrations within both phases are plotted in Fig. 6 as a function of alloy Co content. Superimposed on these plots as solid lines are the equilibrium elemental concentrations of the phases computed at 800 °C using thermodynamic modelling. For each alloy, the thermodynamic modelling predicted the formation of a duplex γ-γ′ microstructure with no additional phases.

The experimental data shown in Fig. 6a indicate that the concentration of Al within the γ phase decreased up to a Co content of ~19 at.% (Ni:Co ratio of 3:1), above which Al concentration increased, inferring a transition in elemental partitioning behaviour at this Ni:Co ratio. Correspondingly, within the γ′ phase, Fig. 6b, an increase in Al concentration was observed initially on addition of Co to the quaternary Ni-Al-Ti-Cr alloy, followed by a decrease in Al concentration as the Co content increased further. The variation in Al concentration with increasing Co content, as predicted by thermodynamic modelling (solid lines in Fig. 6a and b) followed a similar trend, but suggests that the critical Co content at which there is a transition in partitioning behaviour was higher than that found experimentally.

From the Ti partitioning data, Fig. 6c, it can be seen that an increasing Co content (up to ~19 at.%) gave rise to a decrease in the Ti concentration within the γ phase, followed by increased Ti concentration as Co content rose further. This suggests that the observed preferential partitioning to the γ′ phase occurred to a lesser extent at higher Co content. The thermodynamic modelling data (solid line in Fig. 6c) predicted a similar transition in phase

Table 2
Average chemical compositions (at.%) of the γ and γ′ phases and their associated standard deviations in the alloys following ageing at 800 °C for 1000 h, as obtained from the APT proxigram data.

Alloy	Phase	Average composition (at.%)										Partitioning ratio ($C_i^{\gamma'}/C_i^{\gamma}$)									
		Al	±σ	Ti	±σ	Ni	±σ	Cr	±σ	Co	±σ	k_{Al}	±σ	k_{Ti}	±σ	k_{Ni}	±σ	k_{Cr}	±σ	k_{Co}	±σ
0Co	γ	1.77	0.03	1.24	0.03	73.77	0.09	23.23	0.09	–	–	6.15	0.11	9.2	0.2	1.015	0.003	0.124	0.003	–	–
	γ′	10.85	0.07	11.37	0.12	74.9	0.2	2.87	0.08	–	–										
9Co	γ	1.64	0.08	1.00	0.05	60.48	0.18	23.63	0.14	13.25	0.16	6.9	0.4	12.2	0.7	1.180	0.005	0.104	0.005	0.200	0.006
	γ′	11.30	0.16	12.2	0.3	71.39	0.18	2.46	0.11	2.65	0.07										
19Co	γ	1.41	0.08	0.73	0.05	46.75	0.18	24.99	0.08	26.1	0.2	8.0	0.5	16.6	1.1	1.484	0.006	0.080	0.001	0.202	0.004
	γ′	11.27	0.09	12.10	0.05	69.37	0.08	2.00	0.02	5.264	0.104										
28Co	γ	1.74	0.08	0.91	0.07	36.6	0.2	23.82	0.18	36.89	0.18	6.5	0.3	13.49	1.05	1.770	0.011	0.086	0.004	0.260	0.006
	γ′	11.31	0.13	12.22	0.09	64.8	0.2	2.05	0.09	9.6	0.2										
38Co	γ	2.07	0.09	0.95	0.06	25.2	0.3	24.9	0.2	46.8	0.3	5.4	0.3	13.5	0.9	2.28	0.03	0.098	0.004	0.344	0.005
	γ′	11.12	0.19	12.8	0.2	57.5	0.3	2.45	0.09	16.1	0.2										
47Co	γ	3.09	0.18	1.6	0.2	19.8	0.4	21.7	0.3	53.9	0.5	3.3	0.2	7.3	0.9	2.32	0.05	0.173	0.007	0.527	0.009
	γ′	10.26	0.19	11.7	0.3	46.0	0.4	3.75	0.15	28.4	0.4										
56Co	γ	3.72	0.15	2.04	0.18	13.9	0.4	21.2	0.4	59.2	0.4	2.27	0.09	5.9	0.5	2.18	0.06	0.308	0.007	0.723	0.006
	γ′	8.43	0.06	12.0	0.1	30.28	0.15	6.53	0.08	42.79	0.15										

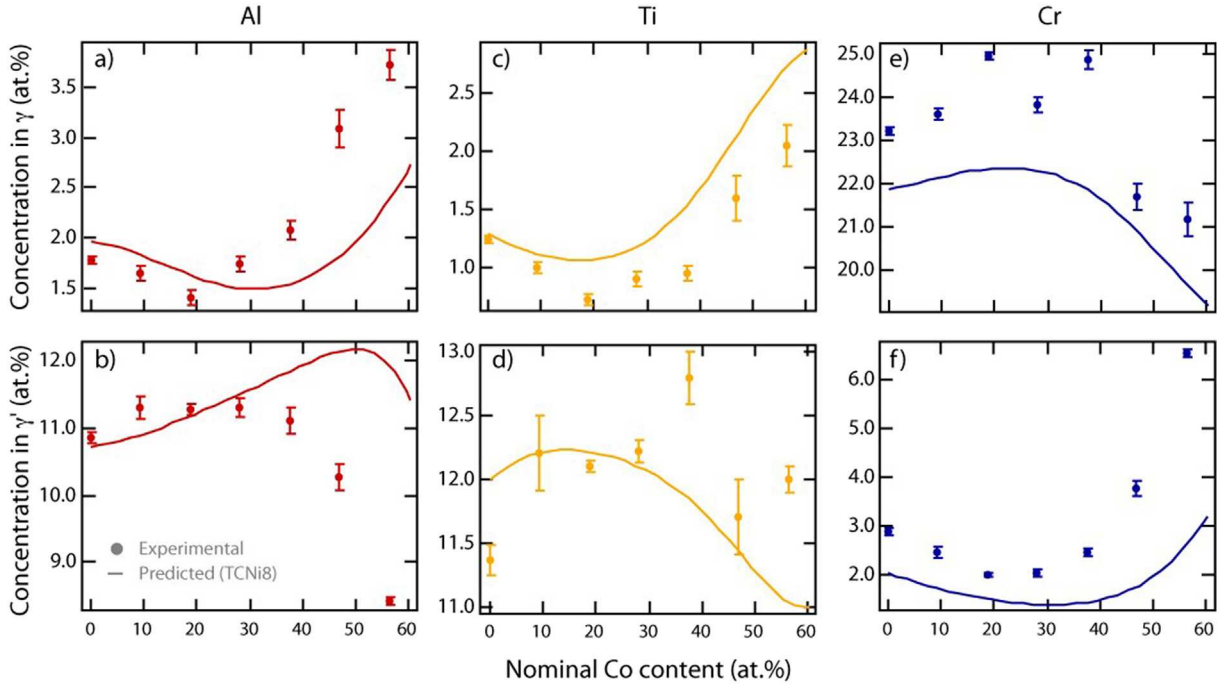

Fig. 6. Concentration of (a) Al in the γ phase; (b) Al in the γ′ phase; (c) Ti in the γ phase; (d) Ti in the γ′ phase; (e) Cr in the γ phase; (f) Cr in the γ′ phase as a function of nominal alloy Co content. Experimental data (markers) are contrasted with thermodynamic predictions (solid lines) obtained using Thermo-Calc with the TCNi8 database for 800 °C.

partitioning behaviour at ~19 at.% Co. However, the concentrations of Ti in the γ phase, as predicted by modelling, were consistently higher than those determined by experiment. For the Ti concentration within the γ′ phase of each alloy, Fig. 6d, experimental data showed no clear correlation between Ti concentration and alloy Co content, whereas corresponding thermodynamic modelling data predicted an increase and then decrease in Ti concentration within the γ′ phase as Co content increased.

With respect to the partitioning of Cr, Fig. 6e indicates that the concentration of Cr within the γ phase increased slightly up to a Co content of ~19 at.%. For alloys with significantly higher Co content, Cr concentration in the γ phase was observed to decrease. Conversely, within the γ′ phase, Fig. 6f, an initial slight decrease in the Cr concentration was observed with increasing Co content (up to ~19 at.%) followed by an increase in Cr concentration as Co content increased further. The modelling data displayed a comparable trend to the experimental data, Fig. 6e and f, though the experimentally-determined Cr concentrations in both the γ and γ′ phases were consistently higher than those predicted using thermodynamic data.

To summarise the experimental data presented thus far, Fig. 7 shows how the elemental partitioning coefficients (k_i) were dependent on the Co content of the alloy. From Fig. 7a, it can be seen that the k_i for Ti was higher than that for Al for each alloy composition tested, with Ti and Al displaying a peak in k_i at a Co content of ~19 at.%. In contrast, Cr exhibited a minimum in the k_i at this critical Co content (~19 at.%), Fig. 7b. Fig. 7c indicates that Ni segregated preferentially to the γ′ phase in the presence of Co and did so to a greater extent with increasing Co additions of up to 47 at.%. Furthermore, it appears that Co partitioned to the γ′ phase to a greater extent as Co concentration in the alloy increased.

Fig. 8 shows the elemental constitution of the two sub-lattices of the γ′ phase as a function of alloy Co content, as predicted by thermodynamic modelling. Fig. 8a and b suggest that, as expected,

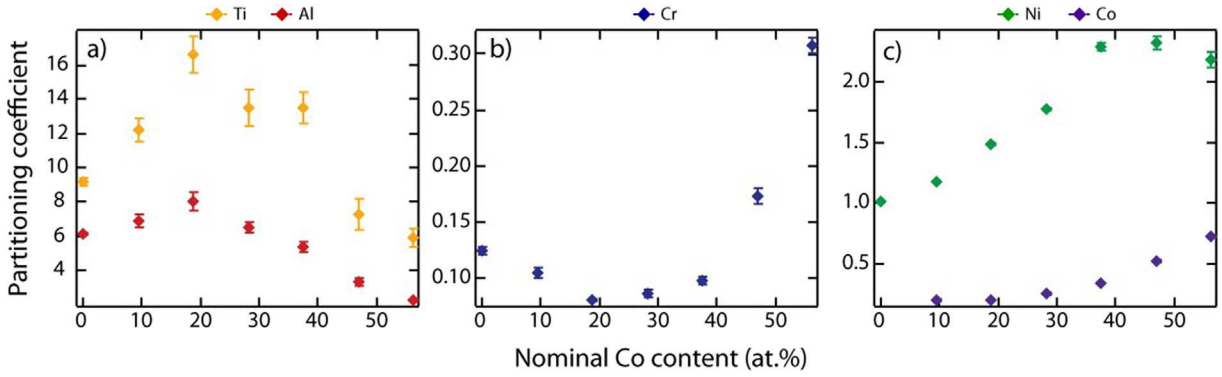

Fig. 7. Variation in elemental partitioning coefficients (k_i) of (a) Al & Ti; (b) Cr and (c) Ni & Co as a function of nominal alloy Co content.

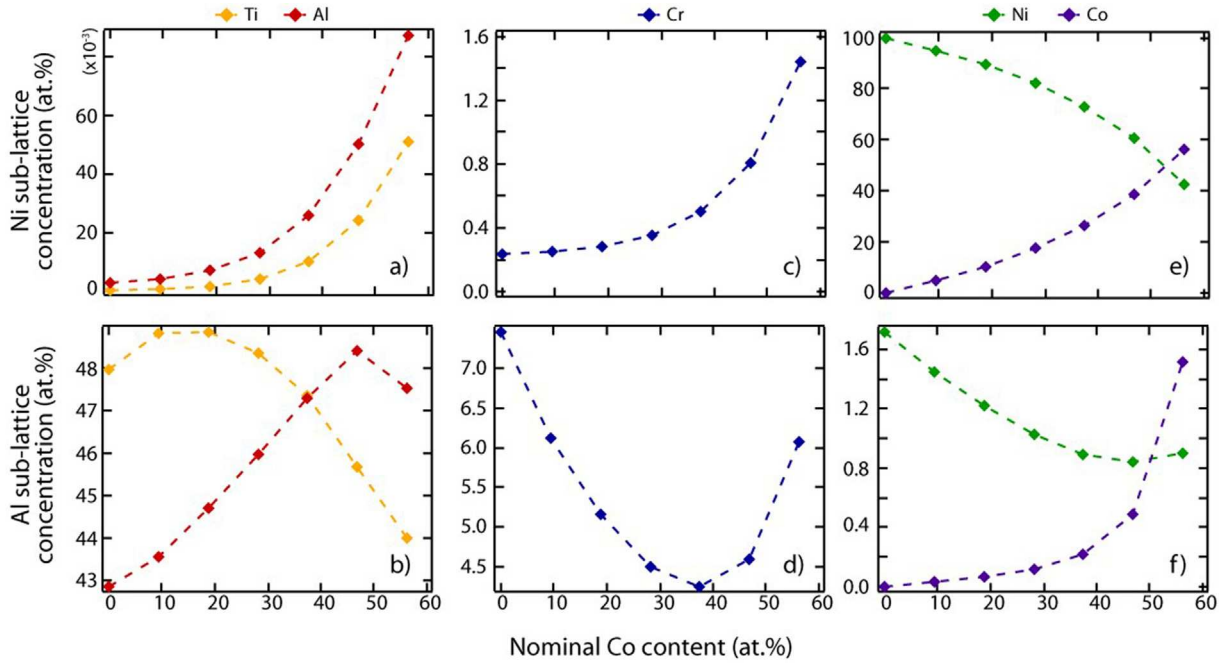

Fig. 8. Concentration of (a) Al and Ti on the Ni sub-lattice; (b) Al and Ti on the Al sub-lattice; (c) Cr on the Ni sub-lattice; (d) Cr on the Al sub-lattice; (e) Ni and Co on the Ni sub-lattice; (f) Ni and Co on the Al sub-lattice with varying alloy Co content, as predicted by Thermo-Calc with the TCNi8 database for 800 °C.

Ti preferentially occupies the Al sub-lattice. A significant fraction of the Cr concentration predicted to reside in the γ′ phase (solid line in Fig. 6f) is anticipated to occupy the Al sub-lattice, Fig. 8c and d. This is suggested by the comparable concentration profiles of Figs. 6f and 8d in addition to the relatively high concentration values calculated for Cr on the Al sub-lattice. Fig. 8e and f would indicate that, for all alloy Co contents, Co substitutes predominantly onto the Ni sub-lattice.

4. Discussion

With increasing Co content in γ-γ′ Ni-Co-Al-Ti-Cr alloys, both Al and Ti were observed to partition more extensively to the γ′ phase up to the Co content of ~19 at.%, after which the preferential segregation of Al and Ti to the γ′ phase was less extensive, Fig. 7a. The inference is that a transition in elemental partitioning behaviour occurs at a critical Co content in the vicinity of 19 at.%. The more extensive degree of partitioning of Al and Ti to the γ′ phase at relatively low Co contents may be attributed to the effect that Co has in reducing the solubility of Al and Ti in the Ni-based γ solid solution [21,23].

In contrast to Al and Ti, with increasing Co additions up to ~19 at.%, the Cr content in the γ phase increased, Fig. 6e, accompanied by a concomitant decrease in Cr concentration in the γ′ phase, Fig. 6f. Increasing concentrations of Cr in the γ phase at relatively low Co content may be due to the increased partitioning of Al and Ti to the γ′ phase, Fig. 6a, c. For alloys with significantly higher Co content, the concentration of Cr in the γ′ phase appeared to increase, Fig. 6f, with a concomitant decrease in the γ phase, Fig. 6e. This suggests that the γ′ phase exhibits a higher solubility for Cr in the presence of high Co concentrations.

The non-monotonic dependence of elemental concentration within the γ and γ′ phases on increasing alloy Co content may be explained with reference to the quaternary phase diagram of the Ni-Co-Al-Ti system derived for the temperature range 750–1100 °C [14,15]. In the Ni-Al rich region of the quaternary phase diagram, the $L1_2$ γ′ phase is likely to be $Ni_3(Al, Ti)$. Where Co and Ti content are increased simultaneously, the effect is to shift the alloy composition across the γ-γ′ two-phase field connecting the Ni-Ni_3Al and Co-Co_3Ti equilibria. This plausibly corresponds to a

gradual chemical shift of the γ′ phase from Ni_3Al-based to Co_3Ti-based [14,15]. The resulting difference in phase chemistry of the γ′ would be expected to induce different elemental phase partitioning in low and high Co variants of alloys from the quaternary Ni-Co-Al-Ti system. Indeed, it has been reported that in γ-γ′ Ni-Co-Al-Ti alloys, a simultaneous decrease in the concentration ratios of Ni:Co and Al:Ti corresponds to marked changes in the partitioning coefficients of Al and Ti on ageing at 750 °C [22]. However, the compositions at which these transitions occurred were not established in that study as a result of the limited number of samples investigated. It has been well established that Ti can substitute extensively for Al in Ni_3Al whereas Co_3Ti exhibits relatively low solubility for ternary alloying elements such as Al [29]. In the current alloys, the transition in elemental phase partitioning behaviour observed with increasing alloy Co content is thus putatively attributed to a change in the solute solubility in the γ′ phase, driven by the underlying thermodynamics of the system.

Despite the preferential partitioning of Co towards the γ matrix phase (k_{Co} consistently <1; Table 2), an increase in the partitioning coefficient of Co was observed with its increasing concentration in the alloy, Fig. 7c. This indicates that the preferential segregation of Co towards the γ phase was occurring to a lesser extent as its concentration in the alloy increased, and that the partitioning of Co toward the γ′ phase was becoming more pronounced. In a recent study published by Oni et al. [22], which examined the atomic site occupancies in γ′ within quaternary Ni-Al-Co-Ti alloys, it was reported that the site preference of Co in the A_3B structure of γ′ changes from a random distribution between the A and B sublattices in the 15 at.% Co alloy to the A sub-lattice with alloy Co content of 30 and 55 at.%. This would indicate that, in Ni-Al-Co-Ti alloys, a chemical transition of the γ′ occurs from Ni_3(Al, Ti) to (Ni, Co)$_3$(Al, Ti) at a critical Co content in the range of 15–30 at.%. Thus, in the current study, it is plausible that at Co contents above ~19 at.%, Co preferentially occupies the Ni sub-lattice of the $L1_2$ structure to form (Ni, Co)$_3$(Ti, Al) and this may underlie the observed phase partitioning behaviour at higher Co contents. However, thermodynamic modelling predicted that the Co partitioning to the γ′ phase substitutes predominantly onto the Ni sublattice *in all alloys*, Fig. 8e and f.

It may be inferred from Fig. 6f that the γ′ phase of alloys comprising Co contents greater than ~19 at.% exhibit rapidly increasing solubility for Cr. With regards to the atomic site preferences of Co and Cr in $L1_2$ Ni_3Al, a first-principles study by Chaudhari et al. [30] suggests that if Co were to reside on the Ni sub-lattice of the γ′ phase, then the most thermodynamically stable atomic configuration would be for Cr to occupy the Al sites of the $L1_2$ lattice. Their study, using density functional theory calculations, indicated that the substitution of Co on to the Ni sub-lattice of the γ′ generates a larger energy barrier for a Cr atom residing on the Al sub-lattice to transfer to the Ni sub-lattice. The implication is that by raising the Co content of the alloy, and with its substitution on to the Ni sub-lattice of the γ′ phase, there is an increase in the thermodynamic driving force for Cr to partition to the Al sites of the Ni_3Al lattice. Furthermore, it has been shown both theoretically and experimentally that in the $L1_2$ Co_3Ti compound, Cr substitutes onto the Ti sub-lattice [10,29]. Thus, it follows that at higher alloy Co contents (above ~19 at.%), Cr may increasingly readily partition to the γ′ phase in which it occupies the (Ti, Al) sub-lattice of (Ni, Co)$_3$(Ti, Al). This is supported by the thermodynamic predictions of atomic site occupancies in γ′, which indicate that the Cr partitioning to the γ′ phase at higher Co content substitutes preferentially for Ti and Al, Fig. 8b, d. This substitution of Cr onto the (Ti, Al) sub-lattice may underlie the observed decrease in the preferential partitioning of Ti and Al to the γ′ with Co contents increasing above ~19 at.%, Fig. 7a.

From Fig. 7c, it is apparent that a Co content of 56 at.% corresponds to a notable decrease in k_{Ni} and to a concurrent increase in k_{Co} that may suggest the onset of a compositional transition of the γ′ from Ni-based to Co-based. It may be inferred from Table 2 that the γ′ phase of alloy 56Co comprises a higher concentration of Co than Ni and is thus Co_3Ti-based. Therefore, it is plausible that, between 47 and 56 at.% Co in the alloy, there is a chemical transition of the γ′ phase occurring from (Ni, Co)$_3$(Ti, Al) to Co_3Ti.

5. Conclusions

Through APT, this study examined the effects that the Ni:Co ratio has on the elemental phase partitioning in alloys from the (Ni, Co)$_{75}$Al$_5$Ti$_5$Cr$_{15}$ alloy system at 800 °C. The following conclusions were drawn.

- All alloys were observed to exhibit a two-phase γ-γ′ microstructure in which Ni, Al and Ti segregated preferentially to the γ′ particle phase (k_i >1) and Cr and Co partitioned preferentially to the γ matrix phase (k_i <1).
- The preferential partitioning of Ti and Al toward the γ′ phase was observed to become greater with an increase in the Co content of the alloy up to ~19 at.%. As the Co content increased above this value, the γ′ solubility for both Ti and Al appeared to decline.
- Cr exhibited a more extensive degree of preferential partitioning toward the γ matrix with increasing Co additions of up to ~19 at.%, above which the preferential segregation of Cr occurred to a lesser extent.
- The non-monotonic correlation observed between elemental phase partitioning and alloy Co content was attributed to a transition in the composition of the γ′ phase from Ni_3(Ti, Al) towards Co_3Ti via (Ni, Co)$_3$(Ti, Al).
- Ni was observed to partition more strongly to the γ′ phase (increasing k_{Ni}) with increasing Co additions of up to 47 at.%. However, Co, whilst always partitioning preferentially toward the γ matrix (k_{Co} <1), did so to a lesser extent with increasing Co content of the alloy (increasing k_{Co}).
- The substitution of Co onto the Ni sub-lattice at higher Co contents (greater than 19 at.%) may be responsible for the apparent increase in Cr substitution onto the Al sub-lattice and concomitant decrease in the solubility of γ′ for Al and Ti, consistent with the thermodynamic data.
- Although predictions of phase compositions based on thermodynamic equilibrium displayed a similar trend to experimental results with respect to phase partitioning in relation to Co content, the absolute values of transition concentrations differed.

Acknowledgements

This work was supported by the Rolls-Royce EPSRC Strategic Partnership under EP/H022309/1 and EP/M005607/1, by the University of Michigan College of Engineering (funding) and by the Michigan Center for Materials Characterization (instruments). The underlying research data can be found at https://doi.org/10.17863/CAM.8774.

Appendix A. Supplementary data

Supplementary data related to this article can be found at http://dx.doi.org/10.1016/j.actamat.2017.03.067.

References

[1] R.C. Reed, The Superalloys, Cambridge University Press, Cambridge, 2006.
[2] R.F. Decker, Strengthening Mechanisms in Nickel-base Superalloys, Steel Strengthening Mechanisms Symposium, Zurich, 1969, pp. 1–24.

[3] T.B. Gibbons, B.E. Hopkins, Creep behaviour and microstructure of Ni-Cr base alloys, Met. Sci. 18 (1984) 273–280, http://dx.doi.org/10.1179/030634584790420104.
[4] N.G. Jones, K.A. Christofidou, P.M. Mignanelli, J.P. Minshull, M.C. Hardy, H.J. Stone, Influence of elevated Co and Ti levels on polycrystalline powder processed Ni-base superalloy, Mater Sci. Technol. 30 (2014) 1853–1861, http://dx.doi.org/10.1179/1743284714y.0000000509.
[5] G.K. Bouse, Eta and platelet phases in investment cast superalloys, in: R.D. Kissinger, D.J. Deye, D.L. Anton, A.D. Cetel, M.V. Nathal, T.M. Pollock, D.A. Woodford (Eds.), Superalloys 1996 (Eighth International Symposium), TMS, 1996, pp. 163–172, http://dx.doi.org/10.7449/1996/superalloys_1996_163_172.
[6] C.Y. Cui, Y.F. Gu, D.H. Ping, H. Harada, T. Fukuda, The evolution of η phase in Ni–Co base superalloys, Mater Sci. Eng. A 485 (2008) 651–656, http://dx.doi.org/10.1016/j.msea.2007.08.047.
[7] J.L. Murray, Co-Ti (Cobalt-Titanium), in: II Ed., in: T.B. Massalski (Ed.), Binary Alloy Phase Diagrams, vol. II, ASM International, 1990, pp. 1250–1252.
[8] P.H. Thornton, R.G. Davies, The temperature dependence of the flow stress of gamma prime phases having the Ll_2 structure, Metall. Mater Trans. B 1 (1970) 549–550, http://dx.doi.org/10.1007/BF02811575.
[9] D.-M. Wee, O. Noguchi, Y. Oya, T. Suzuki, New Ll_2 ordered alloys having the positive temperature dependence of strength, Trans. JIM 21 (1980) 237–247, http://dx.doi.org/10.2320/matertrans1960.21.237.
[10] P. Viatour, J.M. Drapier, D. Coutsouradis, Stability of the γ′-Co_3Ti compound in simple and complex cobalt alloys, Cobalt 3 (1973) 67–74.
[11] P. Viatour, J.M. Drapier, D. Coutsouradis, L. Habraken, Structure and properties of CM-7, a wrought preciptiation-hardening cobalt-base alloy, Cobalt 51 (1971) 67–76.
[12] J.M. Blaise, P. Viatour, J.M. Drapier, On the stability and precipitation of the Co_3Ti phase in Co-Ti alloys, Cobalt 49 (1970) 192–195.
[13] C. Cui, D. Ping, Y. Gu, H. Harada, A new Co-Base superalloy strengthened by γ′ phase, Mater Trans. 47 (2006) 2099–2102, http://dx.doi.org/10.2320/matertrans.47.2099.
[14] C.Y. Cui, Y.F. Gu, D.H. Ping, H. Harada, Phase Constituents Ni–Al–Co–Ti Quaternary Alloys 16 (2008) 910–916, http://dx.doi.org/10.1016/j.intermet.2008.04.006.
[15] V. Raghavan, Al-Co-Ni-Ti (Aluminum-Cobalt-Nickel-Titanium), JPED 30 (2009) 199–200, http://dx.doi.org/10.1007/s11669-009-9492-3.
[16] J.P. Minshull, S. Neumeier, M.G. Tucker, H.J. Stone, A1-$L1_2$ structures in the Al-Co-Ni-Ti quaternary phase system, AMR 278 (2011) 399–404 doi:10.4028/www.scientific.net/amr.278.399.
[17] C. Cui, A. Sato, Y. Gu, H. Harada, Microstructure and yield strength of UDIMET 720LI alloyed with Co-16.9 Wt pct Ti, Metall. Mater Trans. A 36 (2005) 2921–2927, http://dx.doi.org/10.1007/s11661-005-0065-8.
[18] Y. Gu, H. Harada, C. Cui, D. Ping, A. Sato, J. Fujioka, New Ni–Co-base disk superalloys with higher strength and creep resistance, Scr. Mater 55 (2006) 815–818, http://dx.doi.org/10.1016/j.scriptamat.2006.07.008.
[19] Y.F. Gu, C. Cui, D. Ping, H. Harada, T. Fukuda, J. Fujioka, Creep behavior of new kinds of Ni–Co-base superalloys, Mater Sci. Eng. A 510–511 (2009) 250–255, http://dx.doi.org/10.1016/j.msea.2008.04.128.
[20] R.N. Jarrett, J.K. Tien, Effects of cobalt on structure, microchemistry and properties of a wrought nickel-base superalloy, Metall. Trans. A 13 (1982) 1021–1032, http://dx.doi.org/10.1007/bf02643399.
[21] J.K. Tien, R.N. Jarett, Effects of Cobalt in Nickel-base Superalloys, NASA, 1983. Report 168308.
[22] A.A. Oni, S.R. Broderick, K. Rajan, J.M. LeBeau, Atom site preference and γ′/γ mismatch strain in Ni-Al-Co-Ti superalloys, Intermetallics 73 (2016) 72–78, http://dx.doi.org/10.1016/j.intermet.2016.03.006.
[23] J. Heslop, Wrought nickel-chromium heat-resisting alloys containing cobalt, Cobalt 24 (1964) 128–137.
[24] G.E. Maurer, J.A. Domingue, L.A. Jackman, Role of cobalt in waspaloy, in: J.K. Tien (Ed.), Superalloys 1980 (Fourth International Symposium), TMS, 1980, pp. 43–52, http://dx.doi.org/10.7449/1980/superalloys_1980_43_52.
[25] M.V. Nathal, R.D. Maier, L.J. Ebert, The influence of cobalt on the tensile and stress-rupture properties of the nickel-base superalloy MAR-m247, Metall. Trans. A 13 (1982) 1767–1774, http://dx.doi.org/10.1007/bf02647832.
[26] K.A. Christofidou, N.G. Jones, E.J. Pickering, R. Flacau, M.C. Hardy, H.J. Stone, The microstructure and hardness of Ni-Co-Al-Ti-Cr quinary alloys, JALCOM 688 (2016) 542–552, http://dx.doi.org/10.1016/j.jallcom.2016.07.159.
[27] Wavemetrics Igor Pro. Available from: https://www.wavemetrics.com/ [Accessed 23 March 2017].
[28] O.C. Hellman, J.A. Vandenbroucke, J. Rusing, D. Isheim, D.N. Seidman, Analysis of three-dimensional atom-probe data by the proximity histogram, Microsc. Microanal. 6 (2000) 437–444.
[29] Y. Liu, T. Takasugi, O. Izumi, Alloying behavior of Co_3Ti, Metall. Trans. A 17 (1986) 1433–1439, http://dx.doi.org/10.1007/BF02650125.
[30] M. Chaudhari, J. Tiley, R. Banerjee, J. Du, Site preference and interaction energies of Co and Cr in gamma prime Ni_3Al: a first-principles study, Modell. Simul. Mater Sci. Eng. 21 (2013), http://dx.doi.org/10.1088/0965-0393/21/5/055006.